Applied Surface Science 565 (2021) 150552

Contents lists available at ScienceDirect

Applied Surface Science

journal homepage: www.elsevier.com/locate/apsusc

Full Length Article

KPFM and DFT as tools to correlate the charge distribution and molecular orientation of dendritic adsorbates on different surfaces

Eliana D. Farias [a,*], Martin E. Zoloff Michoff [b], Valeria Sueldo Occello [a], Verónica Brunetti [a], Mario C.G. Passeggi (Jr.) [c,d], Thilo Glatzel [e,*]

[a] INFIQC, Universidad Nacional de Córdoba, CONICET, Departamento de Fisicoquímica, Facultad de Ciencias Químicas, Córdoba, Argentina
[b] INFIQC, Universidad Nacional de Córdoba, CONICET, Departamento de Química Teórica y Computacional, Facultad de Ciencias Químicas, Córdoba, Argentina
[c] Laboratorio de Física de Superficies e Interfaces (LASUI), IFIS-Litoral, CONICET y Universidad Nacional del Litoral, Santa Fe, Argentina
[d] Departamento de Física, Facultad de Ingeniería Química, Universidad Nacional del Litoral, Santa Fe, Argentina
[e] Department of Physics, University of Basel, Basel, Switzerland

ARTICLE INFO

Keywords:
Dendrons
Kelvin Probe Force Microscopy
Work Function
π-π stacking interaction
Hydrogen-bonding interactions

ABSTRACT

The interaction between metals and organic layers is currently a hot topic due to its relevance in future applications based on hybrid organic/inorganic systems at the nanoscale. This work studies the surface modification of HOPG and gold substrates by spontaneous adsorption of aryl-dendrons based on either 3,5-bis(3,5-dinitrobenzoylamino) or 3,5-bis(3,5-diaminobenzoylamino) benzoic acids at fully controlled conditions. KPFM is used to assess the local work function variations upon assembly. A correlation between changes in work function values and spatial ordering of the adsorbates is observed. The aryl-dendrons interact with graphite surfaces through π-π stacking, allowing the formation of ordered layers. Due to depolarization effects, these films cause changes in the local work function values that are smaller on graphite surfaces than on gold substrates. Furthermore, the presence of molecular aggregates driven by intermolecular hydrogen bonding for the case of amino functionalized surfaces has a direct impact on the local work function, which varies depending on whether the areas are partially covered or densely packed. DFT calculations were performed in order to gain a deeper understanding of the correlation between the work function variations and the orientation of the effective molecular dipole moment due to the underlying molecular structures of the adsorbed layer.

1. Introduction

Thin films made of organic molecules are extensively used in the fabrication of micro and macroscopic devices such as chemical sensors [1,2], solar cells [3,4], organic field effect transistors [5,6], and organic light emission diodes [7,8]. For instance, in the case of microelectronic devices its applicability relies on the decrease of the work function (WF) of the metal and/or semiconductor contact interfaces, in such a way to facilitate the extraction of electrons from the electrical contacts. The exhaustive control of the electronic properties at the organic layer/metal interface is a key issue in all of these applications, as well as the comprehensive understanding of the chemistry and/or physics behind the occurring phenomena.

The WF of a metal, that is, the energy required to move an electron from the Fermi level of the metal to just outside the solid, has two contributions: one that originates from the bulk chemical potential inside the solid, while the other comes from the electrostatic potential across the interface, also called “surface dipole” [9]. When a molecule is adsorbed on a metallic surface, it can modify the surface WF either via the so-called “pushback or pillow effect” by adding or subtracting the molecular dipole moment to the surface dipole (for molecules with a permanent or induced one), or by transferring charge from the substrate to the molecule or vice versa. While the pushback or pillow effect is always present, the other contribution may or may not occur. These changes of the interfacial properties may depend on several factors, such as molecular orientation or conformation, packaging density, order and disorder, defects in films, and grain boundaries [10,11]. Research in this area extends to different aspects, such as functional groups [12,13], thickness-dependent surface potential related to variations between the lying-down and tilted molecular packing configurations at the interface [14,15], molecular lengths [16], molecular backbones, anchoring groups [17,18], among others.

* Corresponding authors..
E-mail addresses: edfarias@unc.edu.ar (E.D. Farias), Thilo.Glatzel@unibas.ch (T. Glatzel).

https://doi.org/10.1016/j.apsusc.2021.150552
Received 5 February 2021; Received in revised form 25 June 2021; Accepted 3 July 2021
Available online 8 July 2021

Kelvin Probe Force Microscopy (KPFM) is a spatially-resolved and powerful technique to exploit surface potentials and local WF. This technique provides images of the local contact potential difference (CPD), which is the result of minimizing the electrostatic force (or its gradient) between the tip and the sample by applying a *dc*-voltage (V_{dc}) at each image point. Thus the V_{dc} corresponds to the CPD and it is directly related to the WF difference between the tip and the sample [11]. The magnitude of the CPD depends on the tip material and characteristics. However, when different surface regions are investigated with the same probe, the tip potential may be regarded as the CPD reference electrode, which allows the relative comparison of CPD values recorded on two different functionalized regions of a sample. To clarify the scope of the technique, an interesting contribution on this field was reported by Biere *et al.* [19]. By combining high-resolution topographic atomic force microscopy (AFM) data with the simultaneously acquired local WF signal, and considering its dependence with the direction of the molecular dipole moment, they were able to successfully determine the spatial direction of the adsorption of terphenylthiol self-assembled monolayers on *Au*(111) and *Ag*(111) surfaces [19].

Dendrons are the wedged-shaped sections of dendrimers and possess some interesting and useful characteristics. These polymers exhibit structural integrity and homogeneity, with a well-defined internal cavity that has the possibility of encapsulating another molecule, and multiple terminal groups, which favour their interaction with the environment [20]. Similar to dendrimers, dendron molecules present the physicochemical phenomenon known as “the dendritic effect” [21], though from a synthetic point of view are more cost-effective. Surface modification using dendrons offers significant advantages over other polymers, mainly favoured by its properties. For example, dendrons could induce changes on hydrophobicity or hydrophilicity [22] of a surface, making it more biocompatible [23] or improving its response to external stimuli [24,25].

Previously, our group has worked on the adsorption of 3,5-bis (3,5-dinitrobenzoylamino) benzoic acid (*G1-NO_2*) on *HOPG*. The physicochemical and electrical properties of these dendron layers were evaluated by electrochemical techniques [26] and KPFM in air [27]. In a subsequent study, this was extended to a second generation of nitro dendrons (*G2-NO_2*) [28]. Both generations showed the formation of a densely packed monolayer after incubation for a few minutes. More recently, the first generation of the amino dendron (*G1-NH_2*) was studied on *HOPG*, reporting the results comparatively with respect to those of *G1-NO_2* [29]. The differences in the adsorption behaviour were attributed to the *H*-bonding interactions which occur only for the amino derivative [29]. The effect on the WF changes was also evaluated comparatively, presenting opposite effects according to the electron acceptor/donor characteristics of the peripheral groups of the dendrons studied [29].

In the present work, we report the adsorption of *G1-NO_2* and *G1-NH_2* dendrons on *HOPG* and *Au* surfaces under fully controlled conditions, which include low humidity, annealing of the substrate prior to the modification, and an additional heating process post-modification in order to promote migration and reorganization of the films. The surface rearrangement, coverage degree, and dipole layer formation were evaluated by AFM and KPFM techniques. Interestingly, it was found that intermolecular interactions have a great influence on the final results, since they are closely related to the detailed surface distribution of dendrons. Density functional theory (DFT) calculations were also performed to gain additional insight and understanding of the experimental observations.

2. Experimental section

2.1. Materials

G1-NO_2 and *G1-NH_2* dendrons were synthesized following the Kakimoto’s procedure [30,31]. Dendron solutions were prepared immediately prior to their use in dimethylsulfoxide (*DMSO*). Water was purified with a Millipore Milli-Q system. All the reagents are of analytical grade and were used without further purification. Each 10 mm × 10 mm × 1 mm *HOPG* substrate (SPI Supplies) was exfoliated 3 or 4 times, annealed at 520 K for 2 h, and cooled in a nitrogen atmosphere prior to its use. Alumina silicate glass substrates coated with 100 nm thick-*Au* films (purity 99.999%) from Platypus Technologies were also annealed at 520 K for 2 h prior to surfaces modification.

2.2. Surface modification

The *HOPG* samples were prepared inside the N_2 glove-box, where they were cleaved successive times and then underwent a first annealing process. Subsequently, the freshly cleaved and annealed samples were partially incubated in a *DMSO* solution containing 2 mM of either *G1-NO_2* or *G1-NH_2* for 60 min in the pre-chamber of the N_2 glove-box. The derivatized surfaces were then rinsed with copious volumes of ethanol and water, dried under a nitrogen flux, introduced into the N_2 glove-box to ensure an inert and moisture-free atmosphere, and annealed again at 520 K for 2 h. In this way, two distinct regions were generated over the surface of the samples, which were explored: a pristine *HOPG*, called from now on region I, and a dendronized-*HOPG* area pointed out as region II (see Scheme 1). Surface modification of *Au*-coated glass slides were carried out following a similar procedure to that of *HOPG*, but employing incubation times for more than 12 h in order to achieve a complete monolayer [31].

2.3. Instrumentation

AFM and KPFM images were acquired with a commercial Flex-Axiom AFM microscope using a C3000 control electronics system from Nano-Surf and a look-in amplifier HF2 from Zurich Instruments, which served as an external Kelvin controller. All the measurements were carried out in a N_2 glove-box ($H_2O < 0.1$ ppm and $O_2 < 0.1$ ppm). The KPFM images were collected in a single pass mode with amplitude (AM) modulation. In this configuration, both topography and KPFM images, from now on called contact potential difference (CPD) images, were obtained simultaneously using the first and second resonance of the AFM cantilever [11]. For all reported data, we employed a single *Pt/Ir_5*-coated PPP-NCLR cantilever (Nanosensors) with a fundamental resonance frequency of $f_1 = 160$ KHz, which was utilized for the topographic acquisition. The second resonance frequency of the cantilever ($f_2 = 1035$ KHz) was used for KPFM measurements. During image acquisition, the cantilever oscillation amplitude was kept constant by a feedback controller at a set point of 75–85%. In the Flex AFM system both the AC (excitation voltage of 500.0 mV) and DC voltages were applied to the sample so that the WF_S (sample work function) equals the sum of the WF_T (tip work function) and CPD. During KPFM measurements, different regions of the samples were explored by the same tip, thus changes on CPD can be directly associated with variations in the local WF. The processing and analysis of images were done using free software’s Gwyddion® [32] and WSxM [33].

2.4. Theoretical methods

A full conformational search for *G1-NO_2* and *G1-NH_2* was performed using a normal-mode analysis in bond-angle-torsion coordinates followed by an energy minimization with the Dreiding force field, as implemented in the V_{conf} software suit [34]. The two most stable conformers of each dendron were re-optimized at the DFT level using the Becke-Lee-Yang-Parr (B3LYP) functional and a 6-31G(d,p) base, as implemented in Gaussian 09 [35]. A full normal-mode analysis was performed to check that these structures are local minima in the conformational space.

The interaction of the *G1-NH_2* conformers with graphite was explored by means of periodic boundary conditions calculations as

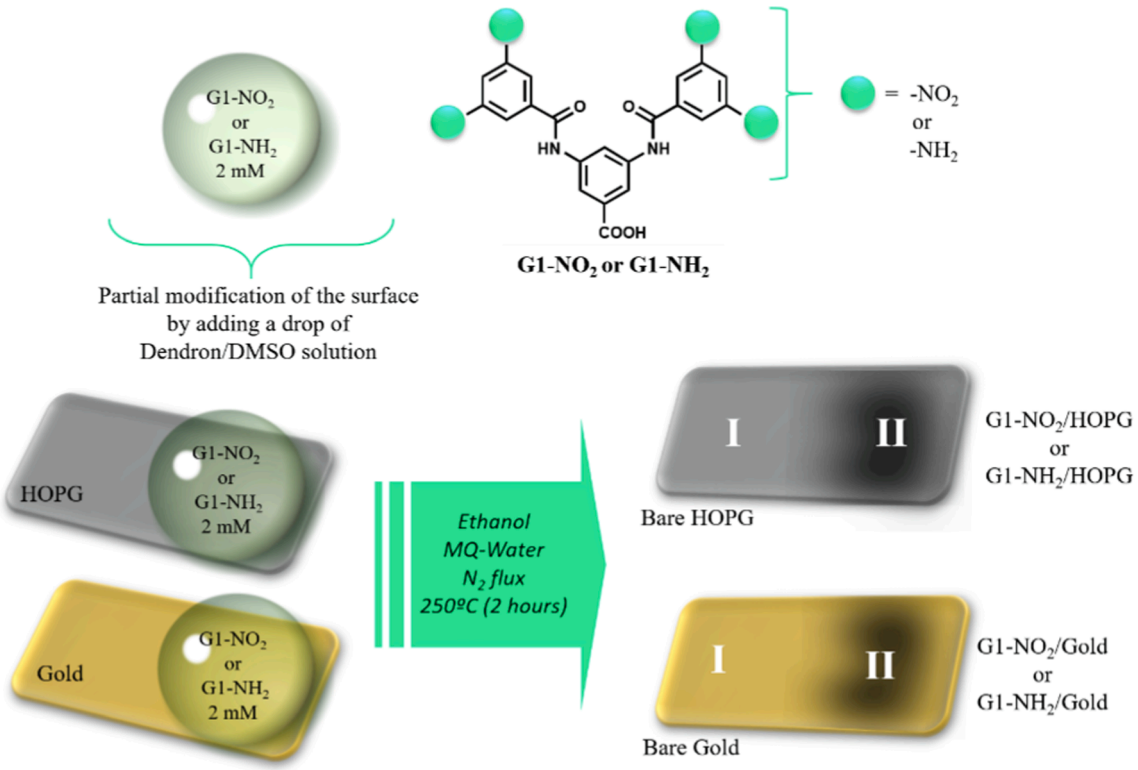

Scheme 1. Schematic drawings of the functionalization of *HOPG* and *Au* surfaces.

implemented in Quantum Espresso [36]. The generalized gradient approximation (GGA) functional developed by Perdew, Burke and Ernzerhof (PBE) [37] in conjunction with projector augmented wave (PAW) pseudopotentials method were employed. Each conformer was adsorbed on graphite, modelled by two 15.6 Å × 28.3 Å (192 atoms) graphene layers and 29.25 Å of vacuum in the direction perpendicular to the surface, in order to avoid spurious interactions between periodic images. For these calculations, cutoff values of 45 Ry (*ca.* 612 eV) and 270 Ry (*ca.* 3673 eV) were used for the plane wave expansion and the electronic density, respectively. The Brillouin zone was sampled employing a 3 × 3 × 1 irreducible Monkhorst-Pack [38] k-point grid. Geometry optimization was performed using the Broyden-Fletcher-Goldfarb-Shanno (BFGS) algorithm with the atoms of the bottom layer fixed. Spin-polarization was considered in all calculations, and Van der Waals interactions were taken into account using a Grimme's DFT-D dispersion method [39]. The simulation cell analysed models a low coverage adsorption situation, in which intermolecular interaction can be neglected.

The change in WF (ΔΦ) and height (h) of the adsorbed molecule on the surface were determined from a single point calculation and using only the Γ-point for the Brillouin zone. A dipole correction in the direction perpendicular to the surface was included in order to compensate for spurious electrostatic interactions. For these calculations, 3 more layers were added to the optimized geometries with 2 layers of graphene, bringing the system to a total of approximately 1000 atoms. Furthermore, the vacuum was also increased to 48.6 Å.

3. Results

3.1. *G1-NO_2 layer*

The adsorption of *G1-NO_2* dendrons on *HOPG,* from exploring the electrochemical behavior through the electro-active nitroso/hydroxylamine couple, was previously reported by our group [26–28]. *G1-NO_2* is physisorbed on the carbon surface favoured by π-π stacking interactions between the aromatic rings of the dendrons and the benzene ring structure of *HOPG* [26,27]. As the adsorption is rapid, leading to the formation of monolayers within a few minutes, a complete dendron layer is expected after the modification process is carried out [26,28]. By applying heat for 2 h in a further annealing process, the reorganization of the dendritic layer leads to the formation of a regular and ordered film, stabilized by adsorbate–adsorbate and adsorbate–substrate π-π stacking interactions.

The topographic and CPD images of different regions of a *HOPG* sample are shown in Fig. 1. In region I, the pristine *HOPG* surface presents the typical structure of terraces separated by steps, some of these terraces are reflected in the CPD image with well-defined edges (Fig. 1a). A slight variation in contrast between the terraces is also observed, probably due to the presence of atmospheric contamination [40]. In region II, a monolayer of *G1-NO_2* dendrons cover entirely and uniformly the surface (Fig. 1b). The typical *HOPG* steps that are perceptible in the topographic image are not observed in the CPD image, where almost the entire surface exhibits the same contrast associated with a similar surface potential. The profile acquired along the black line depicted over a dendrons covered terrace in the image shown in (Fig. 1c) allows us to visualize in a defective discovered area of the film that the dendritic monolayer has a height of (0.8 ± 0.2) nm approximately, in good accordance with the estimated thickness of the layer (see Suppl. Material).

In order to analyse changes in WF upon dendrons adsorption, the histograms acquired from the CPD images of pristine (region I) and *NO_2*-modified *HOPG* (region II) are depicted in Fig. 2(a). Both histograms show no significant differences, thus functionalizing *HOPG* surfaces with nitro-dendrons does not produce any perceptible effects on the surface potential, although it helps to maintain a uniform potential on it, as explained above when analysing CPD images. It should be mentioned, that CPD values herein are different from results previously published by us that showed an increase of 90 mV of the CPD [29]. In our previous work, the layer was prepared by incubation of *HOPG* in 1 mM G1-NO_2/DMSO solution for 15 min, rinsed with ethanol and MQ water, dried by

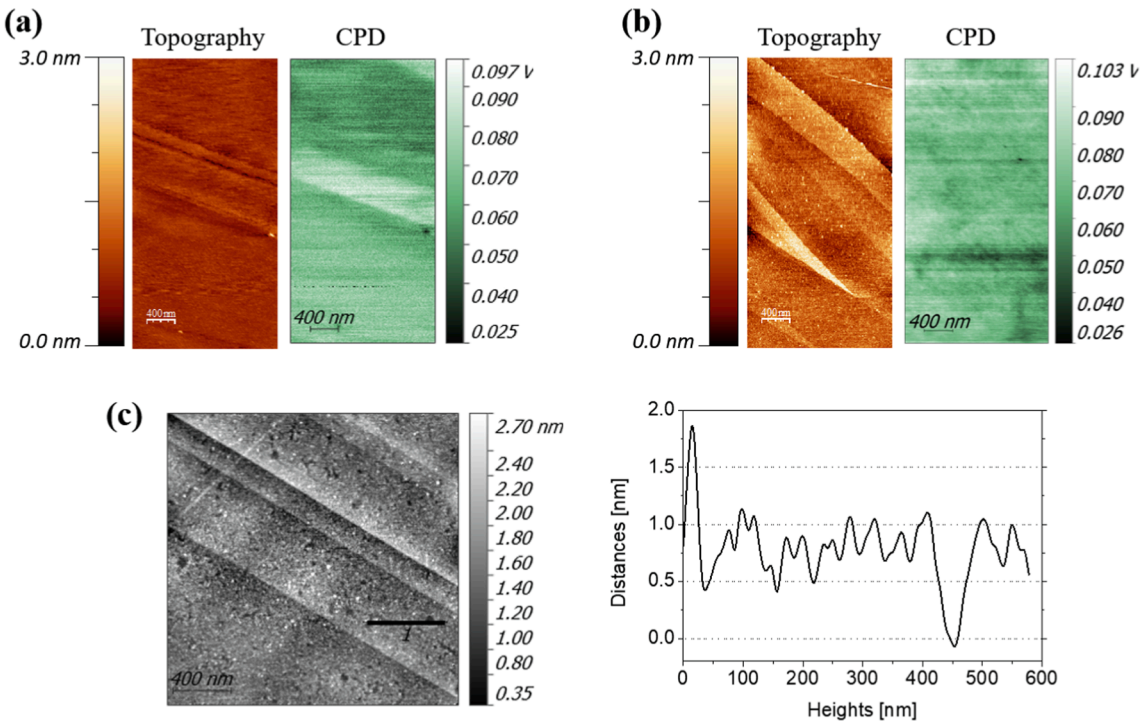

Fig. 1. Topographic AFM and CPD images (2000 nm × 4000 nm) acquired in region I (a) pristine *HOPG*, and region II (b) modified *HOPG* by incubation in a 2 mM *G1-NO$_2$/DMSO* solution for 1 h. (c) Topographic AFM image (2000 nm × 2000 nm) of region II and the corresponding plot of the profile acquired along the line in the image.

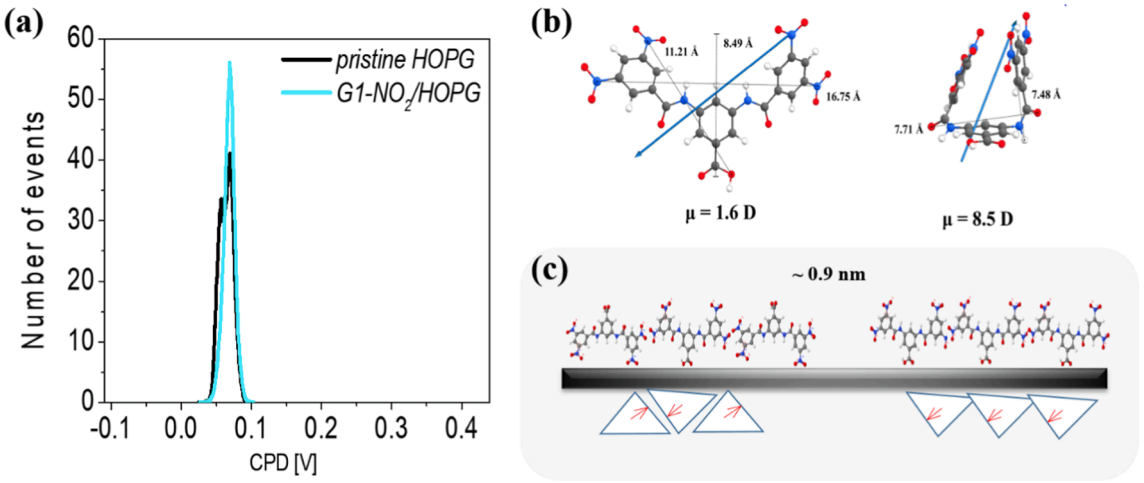

Fig. 2. (a) Histograms obtained from the CPD images shown in Fig. 1(a-b). (b) Schematic drawings of the spatial arrangement of two stable configurations of *G1-NO$_2$* dendrons with their relative distances and dipole moments in vacuum. (c) Possible spatial arrangements of the molecules considering the estimated height of the layer.

N_2-flux and immediately used at atmosphere ambient. In this work, the films are prepared under fully controlled conditions, which include low humidity, annealing of the substrate prior to the modification, and an additional heating process post-modification in order to promote migration and reorganization of the films. Thus, the difference is related to the distribution of the dendrons over the surface. After the annealing process a further reorganized layer is presented and the distribution of its dipole moments changes the substrate work function differently compared to a non-annealed layer.

Two stable configurations of *G1-NO$_2$* molecules were obtained from DFT calculations: one planar or flat extended with a slight twist in one of the arms, and another horseshoe-shaped, which are schematically represented in Fig. 2(b). Some relevant molecular dimensions and the values of the dipole moments assigned for each case in vacuum are also shown. The calculated dipole moment of the planar conformation, which is the energetically most stable conformer, is 1.6 D with a direction almost parallel to the branched line of the molecule, whereas for the horseshoe-shaped conformation, which is 0.45 eV less stable than the planar one, the dipole vector resulted almost perpendicular to the central aromatic of the molecule with a magnitude of 8.50 D.

By considering the height of the dendritic layer estimated from the AFM profile, it can be presumed that dendrons are adsorbed in the planar configuration perpendicular to the surface. Two possible adsorption situations may then occur, which are depicted in Fig. 2(c). The first one is the result of dendron molecules arranged in an inverted way to each other, exposing both nitro and carboxylic groups towards

the dendron/air interface. In this configuration, the z components of the dipole moment practically cancel each other, a situation that would not substantially modify the surface WF. The second configuration exposes only nitro groups to the dendron/air interface. This configuration can then be analysed in terms of a set of dipoles with the negative component pointing towards the *G1-NO_2/HOPG* interface. Since the magnitude of the dipole is rather small, such an arrangement would cause a slight decrease in the superficial WF, a fact that was not observed in the KPFM images. A possible explanation is that the high degree of order of the dendron layer on the surface of *HOPG* leads to a depolarization process, decreasing the effective dipole moment of the molecules, and consequently generating the same effect on the WF [41,42].

The adsorption of *G1-NO_2* dendrons onto *Au* surfaces was previously reported by Paez *et al* [31,43]. The adsorption is not as rapid as in the case of *HOPG* substrates, requiring longer incubation times (overnight) for an effective dendron adsorption. Unlike *HOPG*, *Au* surfaces cannot induce ordering in the dendritic layer because of the absence of π-π stacking interactions between the adsorbate and the substrate. Since dendron molecules should organize on *Au* surfaces only by π-π stacking interactions between neighbouring adsorbates, a comparison among *Au* and *HOPG* substrates raises an interesting question with regards to how the dendron layer structure affects the surface electronic properties.

The topographic AFM and CPD images of bare *Au* (region I) are shown in Fig. 3(a). The clean surface, reconstructed after annealing, presents the typical triangular structures of *Au*(111). The CPD image reflects the edges of the formed structures, presenting a uniform contrast over the terraces. Similarly, Fig. 3(b) shows the topographic AFM and CPD images acquired on region II after the adsorption of *G1-NO_2* dendrons. Although the topography resembles the bare surface, it does not allow differentiating in detail the dendritic monolayer due to the great surface roughness of the sample. On the contrary, the CPD image reveals the WF changes produced by the functionalization of *Au* surfaces. The edges of the minor structures are lost, presenting a surface with a uniform contrast. The histogram from CPD image after dendrons adsorption on *Au* exhibited a maximum shifted *ca. 0.*29 V compared to the corresponding one of bare *Au*. This is indicative of an increase in the WF after adsorption, which can be mainly associated with changes in the surface dipole moment influenced by the presence of an effective dipole moment of the dendritic molecules.

Several configurations can be considered for the adsorption of nitro-dendrons on *Au*. For the case of the planar conformer, three possible geometries are expected: either parallel or perpendicular to the surface and, in the last case, the interaction with the surface can be mediated by the carboxylic or the nitro groups. The component of the dipole moment in the z direction of the first configuration would be very small, rendering a minimal change in the WF. The z component of the dipole moment of the perpendicular geometry would be larger than the previous one, but < 1.6 D. Taking into account the interaction of the carboxylic group, there would be a negative charge density at the *G1-NO_2/Au* interface and a positive charge density at the air/*G1-NO_2* interface, thus causing a decrease in the WF. On the other hand, the charge densities would be inverted for the perpendicular geometry interacting with the nitro groups, causing an increment in the WF. If we consider the horseshoe-like conformation, with a dipole moment of *ca.* 8.5 D in vacuum, the interaction with the surface can be mediated either by the nitro or the carboxylic group and the central ring. The adsorption through the nitro groups would lead to a negative charge build-up at the *G1-NO_2/Au* interface and a positive charge density at the air/*G1-NO_2* interface, thus leading to a rather large decrease in WF, whereas an adsorption through the central ring and the carboxylic group would result in a positive charge density at the *G1-NO_2/Au* interface and a negative charge density at the air/*G1-NO_2* interface, resulting in an increment in the WF.

Notably, it has been reported that p-nitrobenzoic acid interacts with gold surfaces preferably through the oxygen atoms of the carboxylic group [44], which leads us to propose that dendrons adsorption occurs mainly in a horseshoe-like configuration. It has a dipole moment in vacuum greater than 8 D, which causes an increase in the WF, and also stabilizes the structure by π-π stacking interactions between the lateral rings of neighbouring adsorbates.

3.2. *G1-NH_2 layer*

The adsorption of *G1-NH_2* dendrons on *HOPG* was recently reported [29]. *G1-NH_2* is physisorbed on carbon surfaces favoured by π-π stacking interactions between the aromatic rings of the dendrons and the benzene ring structures of *HOPG*. Additionally, the presence of amino groups on the periphery thereof enables *H*-bonding formation between neighbouring adsorbates, leading to compact and ordered regions. This situation is favoured at long incubation times or at high dendron

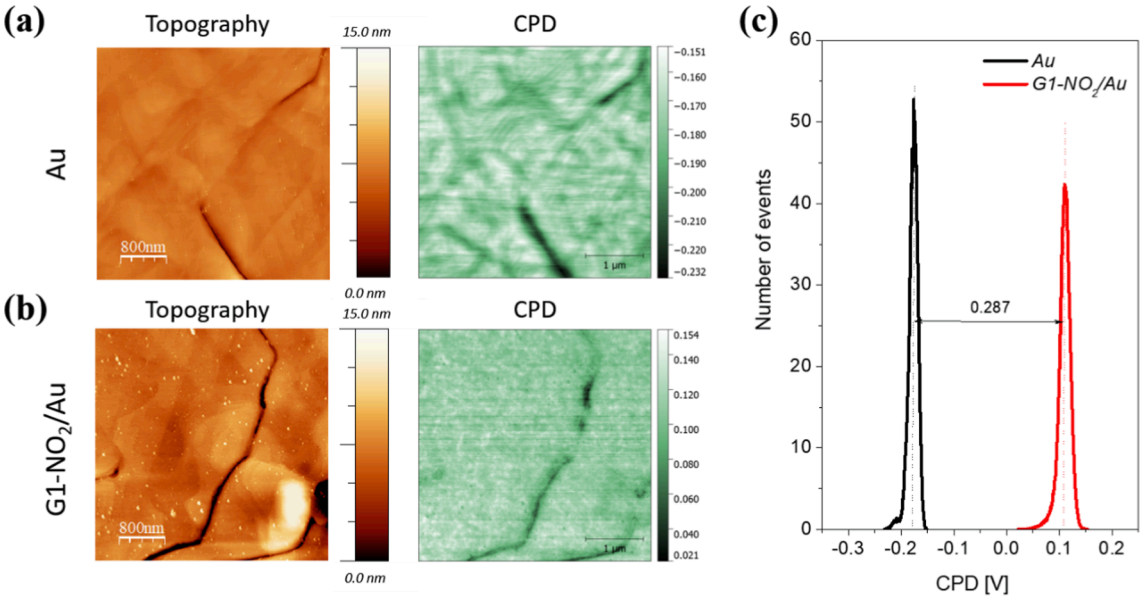

Fig. 3. Topographic AFM and CPD images (4000 nm × 4000 nm) acquired in region I (a) bare *Au* surface and region II (b) modified-*Au* after an overnight incubation in a 2 mM *G1-NO_2/DMSO* solution. (c) Histograms acquired from the CPD images of bare and nitro-modified *Au* regions I and II.

concentrations.

The topographic and CPD images of different regions of a *HOPG* sample, i.e. with and without a *G1-NH$_2$* dendrons modification, are shown in Fig. 4. Region I, corresponding to clean pristine *HOPG*, exhibits a large number of terraces as a result of the sample exfoliation with different contrasts at the edges of the steps in the CPD image, although the terraces present a uniform tone (Fig. 4(a)). Region II, corresponding to the surface modified with amino dendrons, presents areas with different degrees of coverage (Fig. 4(b)). At least three types of quite distinct areas are observed, one which shows a partially covered layer with some isolated deposits (from now on named as sub-region **1**), a second one with structures in the form of interconnected fibbers (sub-region **2**), and finally, the third one showing a fully covered layer (sub-region **3**). The CPD image exhibits distinguished tones for each of the three areas mentioned above. Compact layers (or monolayers) of dendrons present dark contrast in the CPD image, while the brightest one correspond to isolated deposits on the *HOPG* surface. Areas with interconnected fibber-like structures have also a brighter tonality, but intermediate between the other two sectors. The image acquired in high-resolution and its profile taken along the straight line, allows us to visualize in detail the morphologies and heights of each of these three mentioned areas (Fig. 4(c)). While the dendritic compact layer of region **3** presents an estimated height of (0.8 ± 0.2) nm, the neighbouring area (region **2**) formed by the interconnected fibber-like structures presents an average height of (1.1 ± 0.2) nm with some exceptional fibbers of *ca.*1.5 nm. In region **1**, the isolated deposits heights are between 0.8 and 1.6 nm (see additional information in Supplementary Material).

Topographic 3D-AFM images with CPD contrast images overlapped and the corresponding histograms obtained from CPD images of pristine and *G1-NH$_2$*-modified *HOPG* are shown in Fig. 5. The histogram of the surface functionalized with amino dendrons exhibits three maxima associated with the same number of sub-regions over the sample surface, with distinct morphological characteristics already described above. While sub-region **1**, brighter and with a minimum degree of coverage, has the highest CPD values, and sub-region **2** is associated with intermediate CPD values, the most densely populated and compact sub-region **3**, is associated with the lowest CPD values. Sub-region **1** presents the maximum CPD value at 0.380 V, sub-region **2** at 0.309 V, and sub-region **3** at 0.192 V. Pristine *HOPG* surface presents a maximum CPD value at 0.253 V, thus, an increase in the WF of the system after dendronization is observed in sub-regions **1** and **2**, while a decrease is observed in sub-region **3**, related to the densely packed layer.

Therefore, in stark contrast to what was observed for the nitro dendrons, *HOPG* surfaces modified with amino dendrons show significant changes in the superficial WF. Notably, these differences can be correlated with topographic changes of the surface. The main reason behind this observation is most likely related to the coexistence of distinct types of interactions, such as π-π stacking between adsorbate–substrate and/or between adsorbate–adsorbate, and intra or intermolecular *H*-bonding, the latter being a driving force that favours the formation of molecular aggregates, fibbers, or multilayers, even before the formation of the complete monolayer, among others [29].

Fig. 6 shows the average heights associated with the different structures observed in sub-regions **1**, **2**, and **3**, respectively, as a function of the maxima CPD values. The insets show AFM images of each sub-region allowing for a better visualization of the types of structures formed in each case, i.e. fibbers, monolayers, multilayers, or isolated agglomerates.

Similar to *G1-NO$_2$* data, the full conformational search of *G1-NH$_2$* molecules was done and the two most stable configurations are presented in Fig. 6(b). The planar conformation turned out to be more stable than the horseshoe-shaped one by 0.41 eV, where a nitrogen atom mediated *H*-bond has been identified as the main stabilizing factor for this conformer. The calculated dipole moment of the planar conformation is 10.08 D with a direction almost parallel to the central aromatic ring, whereas for the horseshoe-shaped conformation the dipole vector

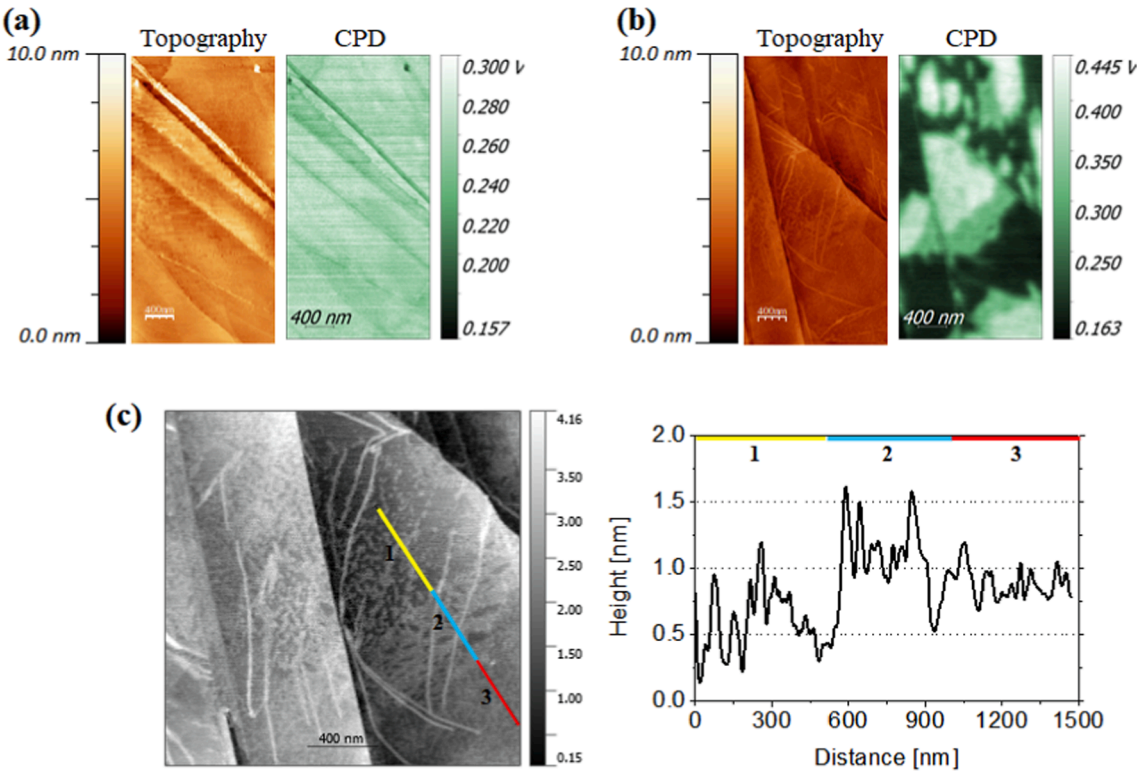

Fig. 4. Topographic AFM and CPD images (2000 nm × 4000 nm) acquired in region I (a) pristine *HOPG* and region II (b) modified *HOPG* by incubation in a 2 mM *G1-NH$_2$/DMSO* solution for 1 h. (c) High-resolution topographic AFM image (2000 nm × 2000 nm) of region II and the corresponding plot of the profile acquired along the straight line in the image.

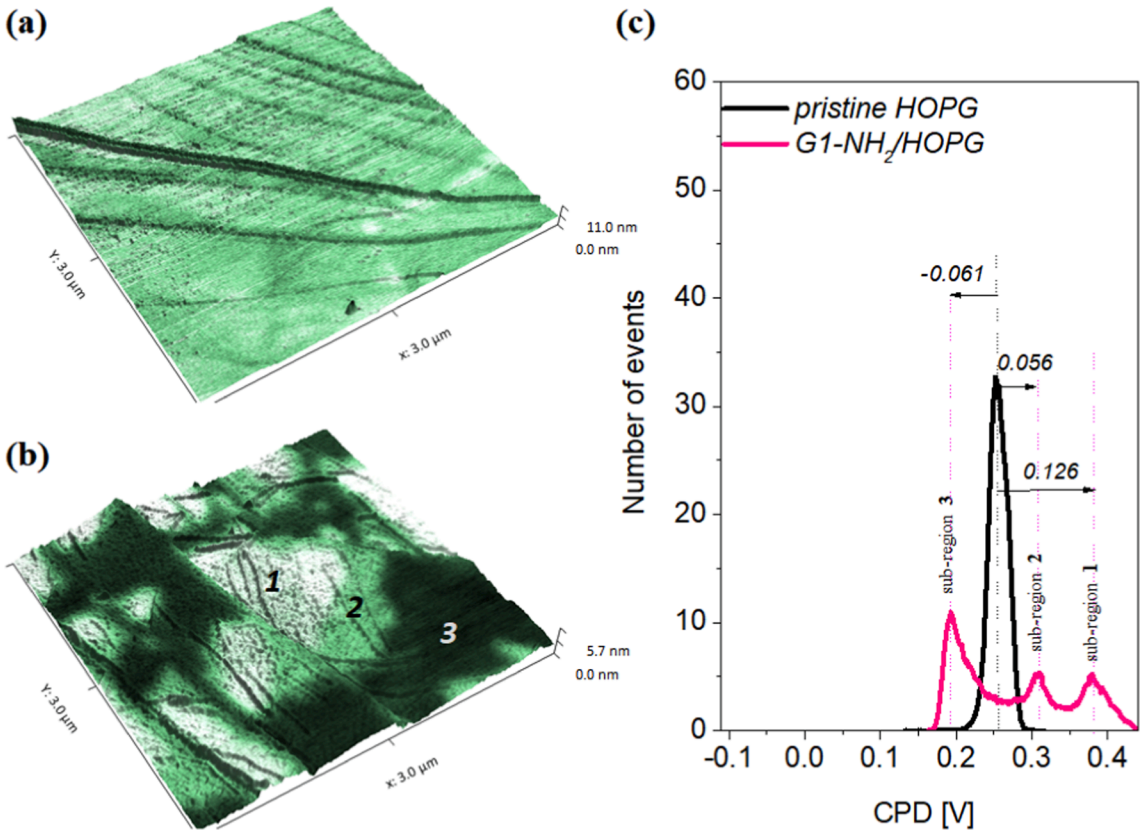

Fig. 5. CPD data overlapped on 3D-AFM images (3000 nm × 3000 nm) of (a) pristine *HOPG* and (b) *G1-NH$_2$*-modified *HOPG*. (c) Histograms corresponding to the statistical analysis of the CPD images of pristine *HOPG* and *G1-NH$_2$/HOPG*. The difference between each peak of the functionalized and pristine *HOPG* surfaces is also indicated.

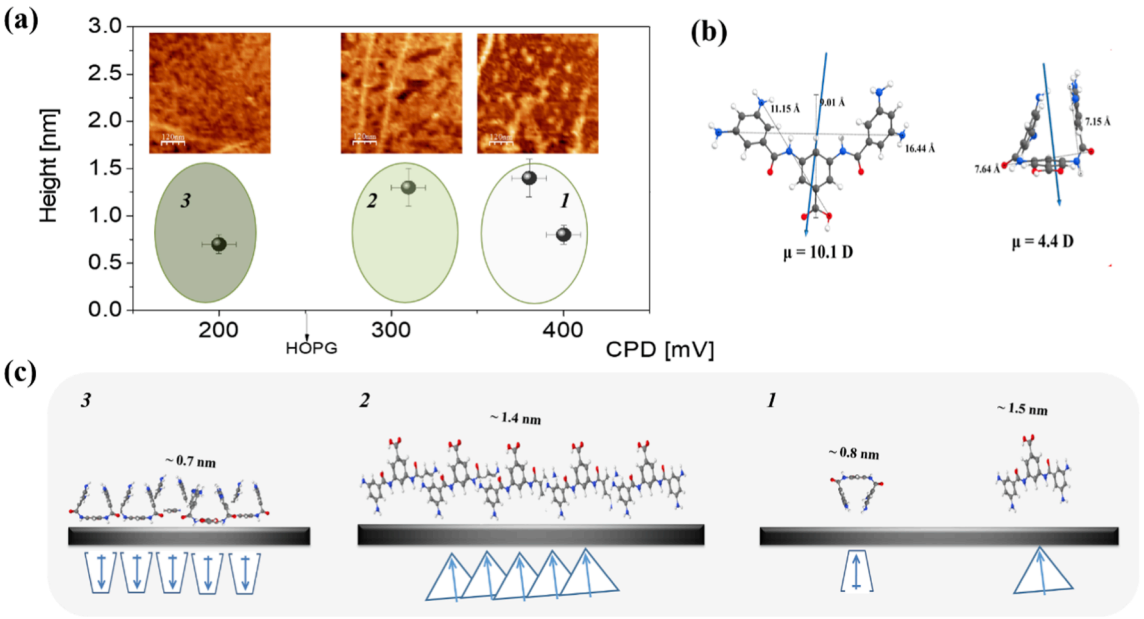

Fig. 6. (a) Average heights of the structures observed in the three different sub-regions of the *G1-NH$_2$/HOPG* surface as a function of the maxima CPD values of each one. Insets: AFM images (600 nm × 600 nm) of each sub-region. (b) Schematic drawings of the spatial arrangement of two stable configurations of *G1-NH$_2$*, with their respective relative distances and dipole moments in vacuum. (c) Possible spatial arrangements of amino-dendrons on *HOPG* considering the average heights of the structures observed in each sub-region.

resulted to be perpendicular to the central aromatic ring of the molecule with a value of 4.40 D. Taking into account the heights in each sub-region and the effect on the WF, different configurations for the adsorption of the *G1-NH$_2$* molecules on the *HOPG* surface are proposed. The sub-region **1** of isolated agglomerates with heights between 0.8 and 1.6 nm can be represented by the configuration schemed in Fig. 6(c)

(right), where the molecules either in their flat or horseshoe structure configurations form the isolated deposits, interacting with the substrate through the amino groups. The increase in the WF implies that the dipole moment of the dendron molecules is larger than the surface dipole moment of *HOPG*, presenting a positive charge density at the *G1-NH$_2$/HOPG* interface and a negative charge density at the air/*G1-NH$_2$* interface. Sub-region **2**, of the interconnected fibber-like structures of *ca.*1.5 nm height, can be represented by the flat or planar vertical structure, as shown in the scheme of Fig. 6(c) (center). Fibber-like structures are favoured by π-π stacking interactions between the aromatic rings of the adsorbates, and also by the formation of *H*-bonding between neighbouring molecules, showing certain anisotropy on the surface of this sub-region. Although the molecular dipole moment contains a significant z-component, depolarization phenomena associated with the order of the layer decreases the effective dipole moment, causing a slight increase in the WF [41,42]. The sub-region **3**, which exhibits a higher degree of ordering, compaction, and structural uniformity, is represented by the adsorption of dendrons in the horseshoe configuration, which exposes the amino groups to air, as shown in Fig. 6 (c) (left). This last configuration is stabilized by π-π stacking interactions between the adsorbates and the substrate, and strengthened by π-π stacking and *H*-bonding interactions between neighbouring adsorbates. The horseshoe structure presents a dipole moment with a negative charge density towards the *G1-NH$_2$/HOPG* interface and a positive charge density at the air/*G1-NH$_2$* interface, leading to a slight decrease in the WF of sub-region **3**.

In order to gain further insight into the possible configurations, the interaction of the two conformers adsorbed on graphene layers, resembling the experimental adsorption of *G1-NH$_2$* molecules onto sub-region **1**, **2**, and **3** of *HOPG* was explored by means of periodic boundary conditions calculations at the DFT level. The simulation cell employed mimics a low coverage adsorption situation, in which molecule–molecule interactions can be neglected. For the horseshoe-shaped conformer the stable adsorption geometry in which the central aromatic ring sits parallel to the surface was analysed (Fig. 7(a)). On the other hand, for the planar conformer two possible adsorption geometries were explored, as shown in Fig. 7(b) and 7(c).

The relative adsorption energies (ΔE_{ads}) for each adsorbate, reported in Table 1, were calculated as the difference in the total electronic energy with respect to the most stable geometry in vacuum conditions, which turned out to be the planar conformer adsorbed parallel to the carbon surface (labelled as (b) in Table 1).

In order to assess the magnitude of the contribution of the dipole arising from molecule-surface charge transfer, Voronoi population analysis on the adsorbates was performed considering the contributions from the molecule and surface. As it can be gathered from the data shown in Table 1, Voronoi population of the molecule and surface for adsorbates (a)-(c), charge transfer from the surface to the molecule is small (in the range of 0.2–0.4 e), thus it is safe to assume that the surface dipole contribution to the work function change is negligible.

Fig. 8 illustrates the changes in the electrostatic potential across the slab. Flat energy regions near the edges correspond to vacuum levels in our model. The zero energy is set at the Fermi level of the system. In this setting, the left-hand-side vacuum-level position is considered the work function of clean graphite (Φ_{graph}). The position of the right-hand-side vacuum-level relative to that of the left one, is the WF change ($\Delta\Phi$) due to the molecule adsorption. It is noteworthy that for our calculations the WF of pristine graphite is *ca.* 4.3 eV, in excellent agreement with values reported in the literature for the same number of layers [45]. The height (h) of the adsorbed molecule is determined as the difference in z between the position of the center of the top-most carbon layer and the region in which the average electronic density is < 0.001 e/Å^3.

Table 1
Difference in adsorption energies (ΔE_{ads}), change in WF ($\Delta\Phi$) with respect to a clean graphite surface, height (h) of the adsorbate for the different geometries studied of the horseshoe-shaped and planar conformers of *G1-NH$_2$* on graphite. Voronoi population of the adsorbates (a)-(c) considered as the contribution from the molecule and the surface.

Adsorbate(*)	ΔE_{ads} [eV] (**)	$\Delta\Phi$ [eV] (***)	h [nm] (****)	Molecule Voronoi Population (#)	Surface Voronoi Population (##)
(a)	1.08	−0.36	0.967	158.4138	3839.5863
(b)	0.00	+0.04	0.520	158.4337	3839.5663
(c)	1.61	+0.57	1.385	158.2077	3839.7906

(*) The labelling corresponds to that of Fig. 7.
(**) Calculated as the difference in electronic energy with respect to the most stable adsorbate, i.e. the planar conformer adsorbed parallel to the surface, see text.
(***) Calculated as the position of the right-hand-side vacuum-level relative to that of the left one, see Fig. 8.
(****) Determined as the difference in z between the position of the center of the top-most carbon layer and the region in which the average electronic density is < 0.001 e/Å^3, see Fig. 8.
(#) The total number of valence electrons for the isolated molecule is 158 (51 atoms).
(##) The total number of valence electrons for the pristine surface is 3840 (960 atoms).

The corresponding values for $\Delta\Phi$ and h for all the adsorbates are summarized in Table I. The electronic density and electrostatic potential profiles for the different adsorbates of the planar conformer are illustrated in Figure S7 of the Supplementary Material. As can be observed, opposite effects are obtained for conformations (a) and (c), similarly to the experimental data obtained from the KPFM images of sub-regions **2** and **3**. Based on the theoretical calculations of adsorbates (a) and (c), as shown in Fig. 7, it is possible to assess different possible configurations for sub-region **1** compatible with the observed WF changes. This sub-region would be composed of isolated aggregates of both configuration (c) for higher heights, and the horseshoe conformer adsorbed in an inverted way with respect to configuration (a) for the lower heights. This is in contrast to sub-regions **2** and **3**, where complete monolayers are observed. Due to the fact that molecules are polarizable, their dipole

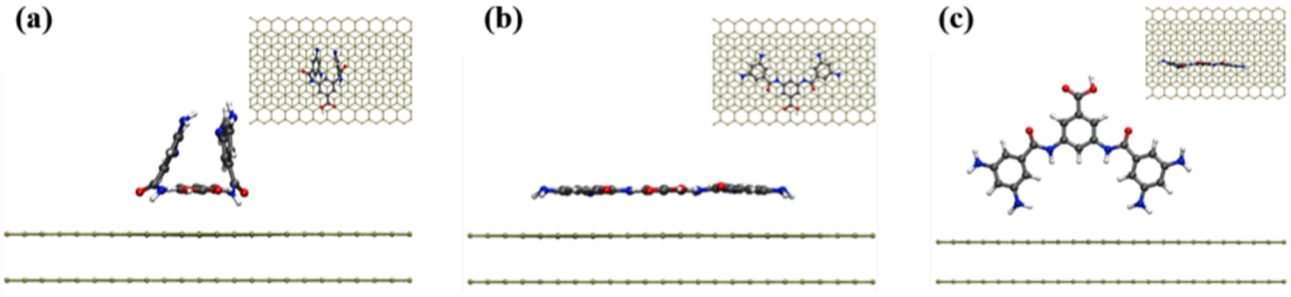

Fig. 7. Top and side views of the optimized structures for different adsorption geometries of *G1-NH$_2$* molecules on graphite. (a) Horseshoe-shaped conformation, (b) planar conformation parallel, and (c) perpendicular to the surface with amino groups point down towards the substrate.

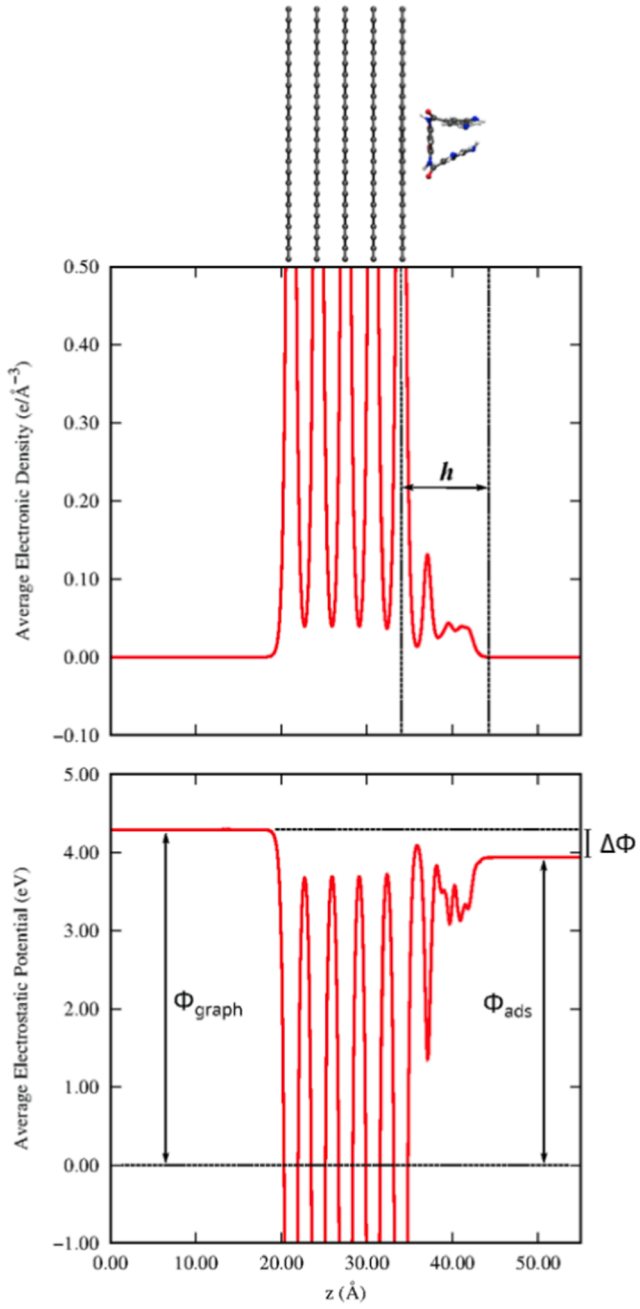

Fig. 8. Horseshoe-shaped conformer on graphite. From top to down, adsorbate geometry, average electronic density, and average electrostatic potential in the direction perpendicular to the surface referred to the Fermi level of the system.

moment can change in response to an external electric field such as that generated by neighbouring molecules. This leads to a partial depolarization when polar molecules are arranged in homogeneous arrays. For instance, Natal *et al.* reported such changes for several molecules, such as aniline, benzene, bromo benzene, and nitro benzene when adsorbed at 0.5 and 1 monolayer with respect to the gas phase [46]. For this reason, marked differences are expected between experimental and theoretical results for the adsorption of *G1-NH$_2$* on *HOPG* in sub-regions **2** and **3**, and less in sub-region **1**.

Topographic AFM and CPD data of bare and amino-dendronized *Au* surfaces are shown in Fig. 9. The reconstructed clean surface obtained after the annealing process, presents the typical triangular structures along with a few circular structures. The CPD image reflects the edges of the polycrystalline *Au* surface, exhibiting a uniform contrast over the terraces. The scanned surface after dendrons adsorption does not reveal any topographic differences attributable to the surface modification, probably due to the fact that a thin layer covers the entire surface, while the CPD image shows a pattern of dark and polydisperse spots. The corresponding histogram exhibits an increase in the CPD value after functionalization the *Au* surface (Fig. 9(c)), showing a light shoulder shifted 0.130 V from bare *Au* related to the isolated spots, and an intense peak shifted 0.169 V associated to the molecular aggregates adsorbed in the rest of the layer surface. The change in the WF is related to the difference in the surface dipole moment, influenced by the presence of *G1-NH$_2$* molecules.

In order to gain a deeper insight into the possible adsorption geometries, the effect on WF is analysed for similar *G1-NH$_2$* conformations as shown in Fig. 7 for HOPG. For the planar conformation adsorbed parallel to the surface, the z component of the dipole moment would be almost negligible, rendering in a very small variation in the WF. When this conformer is adsorbed perpendicular to the surface, interacting through the carboxylic moiety, there would be a negative charge density build-up at the *G1-NH$_2$/Au* interface and a positive one at the air/*G1-NH$_2$* interface, which would cause a decrease of the WF. A perpendicular adsorption through the peripheral amino groups would cause an inverted effect, i.e. an increment in the WF.

On the other hand, if dendrons adsorb through its horseshoe-like conformation, there are two possible adsorption geometries, an interaction through the carboxylic moiety and the central ring, or through the amino functional groups. Following the same reasoning outlined above for the planar conformation, we can conclude that the former adsorption geometry would lead to a decrease in the WF, whereas the latter would cause an increase. Bearing in mind the experimental data presented for *G1-NH$_2$/Au*, both signals may be assigned to *G1-NH$_2$* dendrons adsorbed in the inverted horseshoe-like configuration or in the plane one that interacts via amine groups with the surface. This conformation is stabilized by π-π stacking and *H*-bonding interactions between neighbouring adsorbates, and is also favoured by amino-group interactions with the surface of *Au* [47,48]. The signal assigned to −0.080 V corresponds to islands or compact regions of a molecular height (monolayer), and due to their major order, depolarization processes could reduce the effect over the $\Phi_{substrate}$. The signal assigned to −0.041 V, which corresponds to the background of the CPD image, may be due to the uniform but less ordered adsorption of dendrons. In this case, the depolarization phenomena that tend to decrease the effective surface dipole moment would not have as much weight, causing a greater increase in the WF. Although these conclusions are drawn based solely on the calculated dipole moment of the isolated molecule, previously reported DFT calculations have shown that for structurally similar aromatic molecules the charge transfer upon adsorption on *Au*(1 1 1) is *ca.* 0.4 e [49,50], a similar value to what was found in our study for *G1-NH$_2$* on *HOPG*, thus supporting our conclusions.

4. Conclusions

In the present work, the adsorption of aryl-dendrons based on 3,5-bis (3,5-dinitrobenzoylamino) and 3,5-bis(3,5-diaminobenzoylamino) benzoic acids on highly oriented pyrolytic graphite (*HOPG*) and gold (*Au*) at fully controlled conditions i.e. including low humidity, annealing of the substrate prior to the modification, and an additional heating process post-modification, was investigated by Kelvin probe force microscopy. The rearrangement of the polymeric *G1-NO$_2$* film after the annealing process results in the formation of uniform, ordered, and compact layers of *G1-NO$_2$* dendrons on *HOPG*, stabilized by π-π stacking interactions. Interestingly, *G1-NO$_2$* dendrons are uniformly distributed on *Au* surfaces, but the ordering and magnitude of the interactions between the adsorbates are weaker. The local contact potential difference (CPD) image obtained for the *Au* modified surface reflects these results, although it does not present variations with respect to bare *HOPG*, it shows an increase of the work function (WF). We attribute this

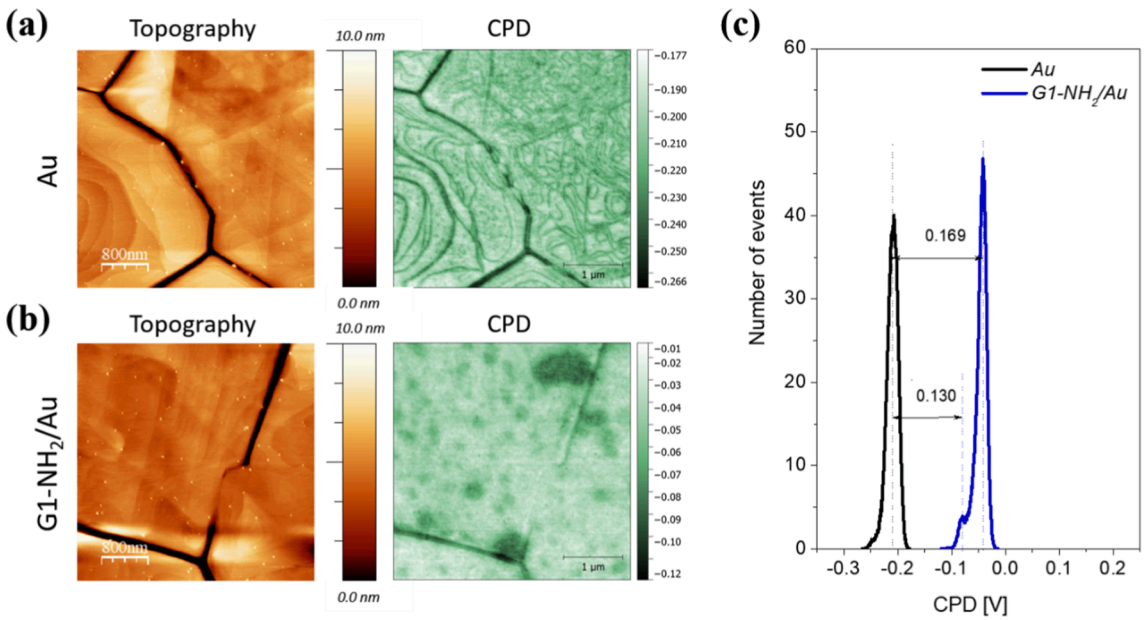

Fig. 9. Topographic AFM and CPD images (4000 nm × 4000 nm) of (a) bare *Au* (region I) and (b) modified-*Au* after an overnight incubation in a 2 m*M G1-NH$_2$/DMSO* solution (region II). (c) Histograms acquired from the CPD images of bare and amino-modified *Au,* regions I and II.

difference to the depolarization events associated with the higher order of adsorption of these molecules on *HOPG* surfaces. The reorganization of the polymeric *G1-NH$_2$* film after the annealing process results in the formation of non-uniform, but ordered layers of *G1-NH$_2$/HOPG*, stabilized by π-π stacking, and *H*-bonding interactions, which favour the formation of dense packed layers and cross-linked fibbers structures. The CPD images are in agreement with this explanation, by decreasing or increasing the WF depending on whether the areas are partially covered or densely packed, respectively. A similar situation was observed for the adsorption of amino-dendron on *Au*, where spots of dense packed layers are associated with changes in CPD, deriving in an increase of the WF. Density functional theory calculations were performed to verify the correlation between the WF variation and the effective molecular dipole moment. The overall results of this work show the importance of controlling the distribution of these dendritic assemblies at a nanoscopic scale to achieve the desired properties on different surfaces.

CRediT authorship contribution statement

Eliana D. Farias: Investigation, Methodology, Writing - original draft. **Martin E. Zoloff Michoff:** Investigation, Writing - original draft, Software. **Valeria Sueldo Occello:** Investigation, Writing - review & editing. **Verónica Brunetti:** Investigation, Writing - review & editing, Writing - original draft, Conceptualization. **Mario C.G. Passeggi (Jr.):** Investigation, Writing - original draft, Writing - review & editing. **Thilo Glatzel:** Investigation, Writing - review & editing, Supervision.

Declaration of Competing Interest

The authors declare that they have no known competing financial interests or personal relationships that could have appeared to influence the work reported in this paper.

Acknowledgements

The authors acknowledge financial support of ANPCyT (PICT 2017-2893) and SECYT-UNC (Res. 411/18). Dr. E. Franceschini and Lic. C. Monzón Somazzi are acknowledged for their valuable contributions in Ellipsometry measurements, and Dr. J.I. Paez and Dr. M.C. Strumia for drendron's synthesis. EDF acknowledge the financial support of Swiss National Science Foundation and the Program International Short Visits (Grant number: IZK0Z2_173501). V.N.S.O. acknowledges the post-doctoral fellowship from CONICET. E.D.F., M.E.Z.M, M.C.G.P., and V. B. are permanent researchers of CONICET. Finally, we all thank the NANOLINO Lab at the Physics Department of Basel University for the use of their SPM equipment, and computational resources from CCAD-UNC, which is part of SNCAD-MinCyT, Argentina.

Appendix A. Supplementary material

Supplementary data to this article can be found online at https://doi.org/10.1016/j.apsusc.2021.150552.

References

[1] B. Lakard, Electrochemical biosensors based on conducting polymers: A review, Applied Sciences. 10 (2020) 6614, https://doi.org/10.3390/app10186614.
[2] E.D. Farias, M.C.G. Passeggi, V. Brunetti, Películas nanoestructuradas de polímeros hiperramificados como plantillas para la formación de estructuras metálicas, Matéria (Rio de Janeiro). 20 (2015) 772–778, https://doi.org/10.1590/S1517-707620150003.0082.
[3] H. Kanda, N. Shibayama, M. Abuhelaiqa, S. Paek, R. Kaneko, N. Klipfel, A. A. Sutanto, C.R. Carmona, A.J. Huckaba, H. Kim, C. Momblona, A.M. Asiri, M. K. Nazeeruddin, Gradient band structure: high performance perovskite solar cells using poly(bisphenol A anhydride- co -1,3-phenylenediamine), J. Mater. Chem. A 8 (2020) 17113–17119, https://doi.org/10.1039/D0TA05496H.
[4] T. Zhu, D. Zheng, J. Liu, L. Coolen, T. Pauporté, PEAI-based interfacial layer for high-Efficiency and Stable Solar Cells Based on a MACl-Mediated Grown $FA_{0.94}MA_{0.06}PbI_3$ Perovskite, ACS Appl. Mater. Interfaces 12 (2020) 37197–37207, https://doi.org/10.1021/acsami.0c09970.
[5] C. Martínez-Domingo, S. Conti, A. de la Escosura-Muñiz, L. Terés, A. Merkoçi, E. Ramon, Organic-based field effect transistors for protein detection fabricated by inkjet-printing, Org. Electron. 84 (2020), 105794, https://doi.org/10.1016/j.orgel.2020.105794.
[6] S. Riera-Galindo, F. Leonardi, R. Pfattner, M. Mas-Torrent, Organic semiconductor/polymer blend films for organic field-effect transistors, Advanced Materials Technologies. 4 (2019) 1900104, https://doi.org/10.1002/admt.201900104.
[7] Z. Xu, B.Z. Tang, Y. Wang, D. Ma, Recent advances in high performance blue organic light-emitting diodes based on fluorescence emitters, J. Mater. Chem. C 8 (2020) 2614–2642, https://doi.org/10.1039/C9TC06441A.
[8] S. Wang, H. Zhang, B. Zhang, Z. Xie, W.-Y. Wong, Towards high-power-efficiency solution-processed OLEDs: Material and device perspectives, Materials Science and Engineering: R: Reports. 140 (2020), 100547, https://doi.org/10.1016/j.mser.2020.100547.
[9] N.D. Lang, W. Kohn, Theory of metal surfaces: Work function, Physical Review B. 3 (1971) 1215–1223, https://doi.org/10.1103/PhysRevB.3.1215.

[10] C. Loppacher, Electronic properties of metal/organic interfaces, in: Springer Series in Surface Sciences (2012) 221–241, https://doi.org/10.1007/978-3-642-22566-6_11.

[11] S. Sadewasser, T. Glatzel, eds., Kelvin probe force microscopy, Springer Berlin Heidelberg, Berlin, Heidelberg, 2012. https://doi.org/10.1007/978-3-642-22566-6.

[12] E. Sauter, C.-O. Gilbert, J.-F. Morin, A. Terfort, M. Zharnikov, Mixed monomolecular films with embedded dipolar groups on Ag(111), The Journal of Physical Chemistry C. 122 (2018) 19514–19523, https://doi.org/10.1021/acs.jpcc.8b04540.

[13] F. Carulli, G. Scavia, E. Lassi, M. Pasini, F. Galeotti, S. Brovelli, U. Giovanella, S. Luzzati, Abifunctional conjugated polyelectrolyte for the interfacial engineering of polymer solar cells, J. Colloid Interface Sci. 538 (2019) 611–619, https://doi.org/10.1016/j.jcis.2018.12.027.

[14] M.C.R. González, P. Carro, L. Vázquez, A.H. Creus, Mapping nanometric electronic property changes induced by an aryl diazonium sub-monolayer on HOPG, PCCP 18 (2016) 29218–29225, https://doi.org/10.1039/C6CP05910D.

[15] W. Xie, J. Xu, J. An, K. Xue, Correlation between molecular packing and surface potential at vanadylphthalocyanine/HOPG interface, The Journal of Physical Chemistry C. 114 (2010) 19044–19047, https://doi.org/10.1021/jp1076565.

[16] A. Szwajca, J. Wei, M.I. Schukfeh, M. Tornow, Self-assembled monolayers of alkylthiols on InAs: A Kelvin probe force microscopy study, Surf. Sci. 633 (2015) 53–59, https://doi.org/10.1016/j.susc.2014.11.023.

[17] M. Gärtner, E. Sauter, G. Nascimbeni, A. Wiesner, M. Kind, P. Werner, C. Schuch, T. Abu-Husein, A. Asyuda, J.W. Bats, M. Bolte, E. Zojer, A. Terfort, M. Zharnikov, Self-assembled monolayers with distributed dipole moments originating from bipyrimidine units, The Journal of Physical Chemistry C. 124 (2020) 504–519, https://doi.org/10.1021/acs.jpcc.9b08835.

[18] D. Cornil, T. Van Regemorter, D. Beljonne, J. Cornil, Work function shifts of a zinc oxide surface upon deposition of self-assembled monolayers: a theoretical insight, PCCP 16 (2014) 20887–20899, https://doi.org/10.1039/C4CP02811B.

[19] N. Biere, S. Koch, P. Stohmann, V. Walhorn, A. Gölzhäuser, D. Anselmetti, Resolving the 3D orientation of terphenylthiol molecules on noble metals with Kelvin probe force microscopy, The Journal of Physical Chemistry C. 123 (2019) 19659–19667, https://doi.org/10.1021/acs.jpcc.9b04982.

[20] D.A. Tomalia, Birth of a new macromolecular architecture: dendrimers as quantized building blocks for nanoscale synthetic polymer chemistry, Prog. Polym. Sci. 30 (2005) 294–324, https://doi.org/10.1016/j.progpolymsci.2005.01.007.

[21] D.A. Tomalia, Dendritic effects: dependency of dendritic nano-periodic property patterns on critical nanoscale design parameters (CNDPs), New J. Chem. 36 (2012) 264–281, https://doi.org/10.1039/C1NJ20501C.

[22] J. Wagner, L. Li, J. Simon, L. Krutzke, K. Landfester, V. Mailänder, K. Müllen, D.Y. W. Ng, Y. Wu, T. Weil, Amphiphilic polyphenylenedendron conjugates for surface remodeling of Adenovirus 5, AngewandteChemie International Edition. 59 (2020) 5712–5720, https://doi.org/10.1002/anie.201913708.

[23] P. Li, W. Zheng, W. Ma, X. Li, S. Li, Y. Zhao, J. Wang, N. Huang, In-situ preparation of amino-terminated dendrimers on TiO_2 films by generational growth for potential and efficient surface functionalization, Appl. Surf. Sci. 459 (2018) 438–445, https://doi.org/10.1016/j.apsusc.2018.08.044.

[24] D. Wu, J. Wu, P. Tao, Y. Yao, J. Wang, D. Liu, F. Chen, B. Xu, W. Li, A. Zhang, Thermoresponsive cationic dendronized copolymers and their corresponding nanogels as smart gene carriers, Polym. Chem. 11 (2020) 4105–4114, https://doi.org/10.1039/D0PY00631A.

[25] E.D. Farias, L.M. Bouchet, V. Brunetti, M.C. Strumia, Dendrimers and dendronized materials as nanocarriers, in: Nanostructures for Novel Therapy, Elsevier (2017) 429–456, https://doi.org/10.1016/B978-0-323-46142-9.00016-5.

[26] J.I. Paez, M.C. Strumia, M.C.G. Passeggi, J. Ferrón, A.M. Baruzzi, V. Brunetti, Spontaneous adsorption of 3,5-bis(3,5-dinitrobenzoylamino) benzoic acid onto carbon, ElectrochimicaActa. 54 (2009) 4192–4197, https://doi.org/10.1016/j.electacta.2009.02.064.

[27] E.D. Farías, V. Brunetti, J.I. Paez, M.C. Strumia, M.C.G. Passeggi, J. Ferrón, Work function maps and surface topography characterization of nitroaromatic-ended dendron films on graphite, Microsc. Microanal. 20 (2014) 61–65, https://doi.org/10.1017/S1431927613013652.

[28] E.D. Farías, J.I. Paez, M.C. Strumia, A.M. Baruzzi, M.C.G. Passeggi (Jr.), V. Brunetti, Self-assembly of the second-generation of nitroaryl-ended dendrons onto carbon, ElectrochimicaActa. 134 (2014) 76–83, https://doi.org/10.1016/j.electacta.2014.04.029.

[29] E.D. Farias, M.C.G. Passeggi, V. Brunetti, Tuning properties of carbon surfaces functionalized with amino-ended dendron layers by exploring their supramolecular interactions, Thin Solid Films 642 (2017) 339–344, https://doi.org/10.1016/j.tsf.2017.10.005.

[30] Y. Ishida, A.C.F. Sun, M. Jikei, M. Kakimoto, Synthesis of hyperbranched aromatic polyamides starting from dendrons as AB_x monomers: Effect of monomer multiplicity on the degree of branching, Macromolecules 33 (2000) 2832–2838, https://doi.org/10.1021/ma992021n.

[31] J.I. Paez, P. Froimowicz, A.M. Baruzzi, M.C. Strumia, V. Brunetti, Attachment of an aromatic dendritic macromolecule to gold surfaces, Electrochem. Commun. 10 (2008) 541–545, https://doi.org/10.1016/j.elecom.2008.01.029.

[32] D. Nečas, P. Klapetek, Gwyddion: an open-source software for SPM data analysis, Open Physics. 10 (2012), https://doi.org/10.2478/s11534-011-0096-2.

[33] I. Horcas, R. Fernández, J.M. Gómez-Rodríguez, J. Colchero, J. Gómez-Herrero, A. M. Baro, WSXM: A software for scanning probe microscopy and a tool for nanotechnology, Rev. Sci. Instrum. 78 (2007), 013705, https://doi.org/10.1063/1.2432410.

[34] C.-E. Chang, M.K. Gilson, Tork: Conformational analysis method for molecules and complexes, J. Comput. Chem. 24 (2003) 1987–1998, https://doi.org/10.1002/jcc.10325.

[35] M. Frisch, G. Trucks, H. Schlegel, G. Scuseria, M. Robb, J. Cheeseman, G. Scalmani, V. Barone, B. Mennucci, G. Petersson, H. Nakatsuji, M. Caricato, X. Li, H. Hratchian, A. Izmaylov, J. Bloino, G. Zheng, J. Sonnenberg, M. Hada, D. Fox, Gaussian 09, Revision A.02, (2009).

[36] P. Giannozzi, S. Baroni, N. Bonini, M. Calandra, R. Car, C. Cavazzoni, D. Ceresoli, G.L. Chiarotti, M. Cococcioni, I. Dabo, A. Dal Corso, S. de Gironcoli, S. Fabris, G. Fratesi, R. Gebauer, U. Gerstmann, C. Gougoussis, A. Kokalj, M. Lazzeri, L. Martin-Samos, N. Marzari, F. Mauri, R. Mazzarello, S. Paolini, A. Pasquarello, L. Paulatto, C. Sbraccia, S. Scandolo, G. Sclauzero, A.P. Seitsonen, A. Smogunov, P. Umari, R.M. Wentzcovitch, QUANTUM ESPRESSO: a modular and open-source software project for quantum simulations of materials, J. Phys.: Condens. Matter 21 (2009), 395502, https://doi.org/10.1088/0953-8984/21/39/395502.

[37] J.P. Perdew, K. Burke, M. Ernzerhof, Generalized gradient approximation made simple, Phys. Rev. Lett. 77 (1996) 3865–3868, https://doi.org/10.1103/PhysRevLett.77.3865.

[38] H.J. Monkhorst, J.D. Pack, Special points for Brillouin-zone integrations, Physical Review B. 13 (1976) 5188–5192, https://doi.org/10.1103/PhysRevB.13.5188.

[39] S. Grimme, Semiempirical GGA-type density functional constructed with a long-range dispersion correction, J. Comput. Chem. 27 (2006) 1787–1799, https://doi.org/10.1002/jcc.20495.

[40] D. Martinez-Martin, R. Longuinhos, J.G. Izquierdo, A. Marele, S.S. Alexandre, M. Jaafar, J.M. Gómez-Rodríguez, L. Bañares, J.M. Soler, J. Gomez-Herrero, Atmospheric contaminants on graphitic surfaces, Carbon 61 (2013) 33–39, https://doi.org/10.1016/j.carbon.2013.04.056.

[41] M.L. Sushko, A.L. Shluger, Dipole−dipole interactions and the structure of self-assembled monolayers, J. Phys. Chem. B 111 (2007) 4019–4025, https://doi.org/10.1021/jp0688557.

[42] M.L. Sushko, A.L. Shluger, Intramolecular dipole coupling and depolarization in self-assembled monolayers, Adv. Funct. Mater. 18 (2008) 2228–2236, https://doi.org/10.1002/adfm.200701305.

[43] J.I. Paez, A.L. Cappelletti, A.M. Baruzzi, V. Brunetti, M.C. Strumia, Preparation, characterization and application of modified surfaces with 3,5-Bis(3,5-dinitrobenzoyl-amino) benzoic acid, Macromolecular Symposia. 290 (2010) 37–45, https://doi.org/10.1002/masy.201050405.

[44] J.J. Panek, A. Jezierska-Mazzarello, A. Koll, G. Dovbeshko, O. Fesenko, p-Nitrobenzoic acid adsorption on nanostructured gold surfaces investigated by combined experimental and computational approaches, ChemPhysChem 12 (2011) 2485–2495, https://doi.org/10.1002/cphc.201100067.

[45] E.V. Rut'kov, E.Y. Afanas'eva, N.R. Gall, Graphene and graphite work function depending on layer number on Re, Diam. Relat. Mater. 101 (2020), 107576, https://doi.org/10.1016/j.diamond.2019.107576.

[46] A. Natan, L. Kronik, H. Haick, R.T. Tung, Electrostatic properties of ideal and non-ideal polar organic monolayers: Implications for electronic devices, Adv. Mater. 19 (2007) 4103–4117, https://doi.org/10.1002/adma.200701681.

[47] R. Holze, The adsorption of aniline on gold: a SERS study, Journal of Electroanalytical Chemistry and Interfacial, Electrochemistry. 250 (1988) 143–157, https://doi.org/10.1016/0022-0728(88)80199-2.

[48] R.C. Hoft, M.J. Ford, A.M. McDonagh, M.B. Cortie, Adsorption of amine compounds on the Au(111) surface: A density functional study, The Journal of Physical Chemistry C. 111 (2007) 13886–13891, https://doi.org/10.1021/jp072494t.

[49] C. Li, S. Monti, X. Li, Z. Rinkevicius, H. Ågren, V. Carravetta, Theoretical study of para-nitro-aniline adsorption on the Au(111) surface, Surf. Sci. 649 (2016) 124–132, https://doi.org/10.1016/j.susc.2016.01.008.

[50] M.L. Para, O.E. Linarez Pérez, M.I. Rojas, M. López Teijelo, Experimental and vdW-DFT study of the structure properties, and stability of isonicotinic acid self-assembled monolayers on gold, The Journal of Physical Chemistry C. 120 (2016) 4364–4372, https://doi.org/10.1021/acs.jpcc.5b11146.